Layout of CCS monitoring infrastructure with highest probability of detecting a footprint of a CO_2 leak in a varying marine environment

Hilde Kristine Hvidevold [a], Guttorm Alendal [a,b,*], Truls Johannessen [c,d], Alfatih Ali [a], Trond Mannseth [e,a], Helge Avlesen [b]

[a] University of Bergen, Department of Mathematics, Allegaten 41, 5008 Bergen, Norway
[b] Uni Research Computing, Bergen, Norway
[c] University of Bergen, Geophysical Institute, Bergen, Norway
[d] Uni Research Climate, Bergen, Norway
[e] Uni Research CIPR, Bergen, Norway

ABSTRACT

Monitoring of the marine environment for indications of a leak, or precursors of a leak, will be an intrinsic part of any subsea CO_2 storage projects. A real challenge will be quantification of the probability of a given monitoring program to detect a leak and to design the program accordingly. The task complicates by the number of pathways to the surface, difficulties to estimate probabilities of leaks and fluxes, and predicting the fluctuating footprint of a leak. The objective is to present a procedure for optimizing the layout of a fixed array of chemical sensors on the seafloor, using the probability of detecting a leak as metric. A synthetic map from the North Sea is used as a basis for probable leakage points, while the spatial footprint is based on results from a General Circulation Model. Compared to an equally spaced array the probability of detecting a leak can be nearly doubled by an optimal placement of the available sensors. It is not necessarily best to place the first in the location of the highest probable leakage point, one sensor can monitor several potential leakage points. The need for a thorough baseline in order to reduce the detection threshold is shown.

© 2015 The Authors. Published by Elsevier Ltd. This is an open access article under the CC BY license (http://creativecommons.org/licenses/by/4.0/).

1. Introduction

If carbon capture and storage (CCS) should be considered a safe and reliable option for mitigating the increasing levels of CO_2 in the atmosphere, it is important to assure that each storage site keeps a major part of the CO_2 isolated and away from the atmosphere for decades (Haugan and Joos, 2004). If not, the decreasing effectiveness of the power plants with CCS might lead to increased CO_2 releases; the opposite of the scope.

The EU directive 2009/31/EC establishes a legal framework for geological storage, eliminating as far as possible negative effects and environmental risks associated with geological storage operations, aligned with the amendments to the 1996 London Protocol and to the OSPAR Convention. An important part of the imposed requirements is an adequate monitoring program.

This monitoring program has three main objectives; (1) assure that a leak will likely be detected, (2) continue to build an accurate baseline to capture trends and natural variability, and (3) to prevent unjustified accusations of adverse effects from the storage project. The 2011 incident at the Weyburn project is an example of the latter (Boyd et al., 2013).

CO_2 injected into geological formations will be buoyant and tend to rise (Nooner et al., 2006). A number of different trapping mechanisms will keep the injected CO_2 in the formation (Rutqvist, 2012). With proper selection and operational procedures a storage project will be designed not to leak. The injection well will be, both during and after injection, the most probable leak pathway and it must be monitored. Rise of CO_2 through the well will be detected and a countermeasure mobilized.

However, the transport of the CO_2 within the formation might cause other pathways to the surface to become probable, or the CO_2 might create new pathways (Oldenburg and Lewicki, 2006). Such pathways can be other wells or structures perforating the cap rock. If the CO_2 rises to shallower formations, other pathways might cause a leak far away from the injection site.

* Corresponding author at: University of Bergen, Department of Mathematics, Allegaten 41, 5008 Bergen, Norway. Tel.: +47 55584044; fax: +47 55582838.
E-mail address: guttorm.alendal@math.uib.no (G. Alendal).

Even if the formation is monitored and the bulk part of the CO_2 plume is followed from year to year, there will be uncertainties on the quantification of CO_2 contained within the formation. Further, what is the detection limit of CO_2 migrating toward the surface and do we know all the potential pathways to the surface?

The CO_2 will rise through the water column either as liquid droplets deeper than $\sim$500 m, or gas bubbles shallower than $\sim$ 500 m (Alendal and Drange, 2001). In the shallow regime a seep will create individual bubbles, bubble trains, or bubble plumes if the flux rate is high enough. The dynamics of these regimes are different, with the plume dynamics being the most challenging to model. Detection of bubbles can be made from sonars (Brewer et al., 2006; Noble et al., 2012). It will be necessary to distinguish between natural seeps and seeps originating from the storage site.

An increase in CO_2 concentration is expected in the vicinity of a leak, with potential environmental impacts (Blackford et al., 2010). Environmental changes might serve as indicators that a leak is occurring, especially through changes in bottom fauna such as new occurrences of bacterial mats (Wegener et al., 2008).

A statistical baseline of important environmental parameters, e.g. currents, natural gas seeps and biogeochemical parameters, is required for designing a comprehensive monitoring program. Historical data are important in combination with new data collected during site characterization. Long time series are important in order to capture natural variability, such as seasonal changes and long term trends. A monitoring program should be designed with this in mind. In particularly it will be important to capture the expected increase of CO_2 concentration caused by the acidification of marine waters (Caldeira and Wickett, 2003).

The main objective is to demonstrate use of a baseline to design a layout of sensors to detect a leak in a given area. The design is based on (1) identification of possible seep locations, (2) characteristics of seepage to the water column and (3) the ability to detect elevated CO_2 concentrations. Section 2 describes implementation of the environmental statistics to optimize the design, and the simplifications and assumptions made in this study. The results is presented in Section 3 and discussed in Section 4.

2. Methods

The procedure relies on answering three main questions; where will a leak most likely occur, how will a leak appear and can a leak be detected?

2.1. Identifying leakage pathways and leak scenarios

Identification of possible pathways to the seafloor, and estimated likelihood of mobilization of any of these, will be part of the required site characterization (EU Commission, 2011). This survey makes it possible to define leak scenarios needed for the required impact and risk assessments.

The site specific spatial and temporal evolution of the CO_2 plume within the storage formations determines the area to be monitored. The anisotropic evolution of the Sleipner plume (see e.g. Boait et al. (2012)) illustrate that subsurface monitoring is a prerequisite for designing a marine monitoring program. The 5-year review of the monitoring program, as required by the EU directive, should be made through best available knowledge at the time.

2.1.1. The simplified leak scenarios used in this study

A proper assessment of possible leakage pathways in the North Sea is not available for this study, nor is it the scope to perform a detailed site specific design. A publicly available map (Norwegian Petroleum Directorate, 2014), locating wells and faults in a 77 km × 77 km area close to Sleipner, is used as an example (Fig. 1).
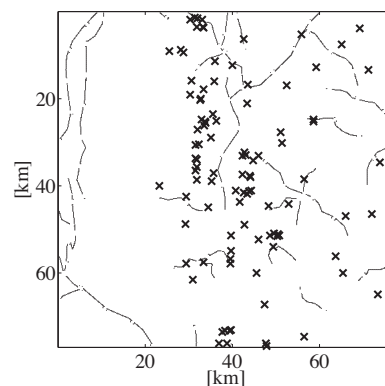

Fig. 1. A (77 × 77) km area in the North Sea, showing the locations of wells (black crosses) and faults (black lines), taken from NPD webpage Norwegian Petroleum Directorate (2014).

Taken from NPD webpage Norwegian Petroleum Directorate (2014).

The areas in the vicinity of wells and faults are assumed to have the highest probability for being the location of the leak. Since CO_2 might also migrate in the lateral direction during ascent, the vicinity of a well or formation have a probability leveling off as function of distance, i.e., assumed to be

$$p(x) = e^{-\left(\frac{x-x_0}{\sigma}\right)^2},\qquad(1)$$

away from x_0, the location of the well/fault. The value $\sigma = 0.2$ m is used in this study.

Due to lack of suitable data it is assumed that each well has the same probability of being the location of a leak, with a similar assumption on faults but then with a four times lower probability compared to wells. To distinguish between wells or faults reaching the storage formation, and those who do not, will require a thorough characterization of the underburden.

To account for potential unknown pathways a low background probability is added to the map. Under the assumption that a leak is ongoing within the area the map of probabilities is normalized i.e., the probability that a leak occurs is 1.

2.2. Predicting the footprint of a leak

The most dominant process during bubble seeps is interfacial drag between bubbles and seawater, retarding the bubble velocity and creating a lifting force acting on the carrier phase. Simultaneously the CO_2 gas within the bubble will be dissolved into the surrounding water, causing density increase and negatively buoyant water masses. Simulating the dynamically active zone is challenging, especially due to the many different scales that are involved, ranging from 10^{-2} m (bubble scale) to 10^2–10^3 m (scale of dynamically active concentration field) (Alendal and Drange, 2001; Dewar et al., 2013, 2014). Away from the dynamically active zone the CO_2 concentration behaves as a passive tracer, being transported and further mixed by local currents and turbulence. Locally there might be strong variations in current conditions and mixing, influenced by a number of factors such as surface wind, tide (Davies and Furnes, 1980) and topography (Alendal et al., 2005). A thorough statistical baseline of environmental conditions will enable reliable prediction of the spatial and temporal characteristics of a CO_2 footprint.

2.2.1. Simulating the CO_2 footprint

The simplified footprint prediction used accounts for the tidal ellipse (Davies and Furnes, 1980) and the local large scale circulation. An 800 m resolution regional ocean model (Bergen Ocean

Model; BOM) set-up for the North Sea advects and disperse CO_2 as a passive tracer (Alendal et al., 2013).

The model forcing comprises tide (four tidal constituents; M_2, S_2, K_1, and N_2), river runoff data, and initial and lateral boundary conditions for salinity and temperature taken from the UK Metoffice FOAM 7 km model published at (http://www.myocean.eu/). The atmospheric forcing is based on spring 2012 data, collected and interpolated from The European Centre for Medium-Range Weather Forecasts (ECMWF, the Centre). In the vertical 41 sigma-coordinate layers is used, distributed with higher resolution (1 m) near the free surface and the sea floor.

The standard model is extended with an additional passive tracer equation, the CO_2 concentration, advected and diffused through the standard equation:

$$\frac{\partial C}{\partial t} + \vec{U} \cdot \nabla C = \frac{\partial}{\partial z}\left(K_H \frac{\partial C}{\partial z}\right) + \frac{\partial}{\partial x}\left(A_H \frac{\partial C}{\partial x}\right) + \frac{\partial}{\partial y}\left(A_H \frac{\partial C}{\partial y}\right) + Q, \tag{2}$$

where C is the CO_2 concentration, $\vec{U} = (U, V, W)$ is the velocity vector in Cartesian x-, y- and z-coordinates, with w being the vertical component. The horizontal and vertical diffusivity coefficients are A_H and K_H, respectively, using turbulence closure scheme from Mellor and Yamada (1982). The last term, Q, is a source term for CO_2. In this study the source term represent a leak rate of 1 kg/s being dissolved over the volume (800 m $\times$ 800 m $\times$ 1 m) located closest to the seabed, i.e. the grid-cell closest to the seafloor.

As a further simplifications the constant leakage rate and the resulting sea floor concentration average, shown in Fig. 2a, are independent on leak location. In reality flux will be dependent on leak location, and might even be time dependent, and local topography and current variability might alter the characteristics. For a better description seasonal, spatial variability and long term trends will have to be accounted for. This will require availability of the aforementioned current statistics and a much more comprehensive simulation study.

2.2.2. Determining the most probable footprint

The average seafloor concentration is sought to be approximated by a function

$$c = \boldsymbol{G}(\boldsymbol{x}; \boldsymbol{z}) = c_0 e^{(-(\boldsymbol{x}-\boldsymbol{x}_0)^T \boldsymbol{A}(\boldsymbol{z})(\boldsymbol{x}-\boldsymbol{x}_0))}. \tag{3}$$

with the matrix

$$\boldsymbol{A}(\boldsymbol{z}) = \begin{bmatrix} \dfrac{\cos^2\theta}{2\sigma_x^2} + \dfrac{\sin^2\theta}{2\sigma_y^2} & -\dfrac{\sin 2\theta}{4\sigma_x^2} + \dfrac{\sin 2\theta}{4\sigma_y^2} \\ -\dfrac{\sin 2\theta}{4\sigma_x^2} + \dfrac{\sin 2\theta}{4\sigma_y^2} & \dfrac{\sin^2\theta}{2\sigma_x^2} + \dfrac{\cos^2\theta}{2\sigma_y^2} \end{bmatrix}, \tag{4}$$

a parameter vector $\boldsymbol{z} = [\theta, \sigma_x, \sigma_y]$, maximum concentration, c_0, at the leakage location, $\boldsymbol{x}_0$, and $\boldsymbol{x}$ is the position vector.

For a given constant c_t,

$$c_t = \boldsymbol{G}(\boldsymbol{x}; \boldsymbol{z}) = c_0 e^{-((\boldsymbol{x}-\boldsymbol{x}_0)^T \boldsymbol{A}(\boldsymbol{x}-\boldsymbol{x}_0))}, \tag{5}$$

leads to

$$\ln \frac{c_0}{c_t} = (\boldsymbol{x}-\boldsymbol{x}_0)^T \boldsymbol{A}(\boldsymbol{x}-\boldsymbol{x}_0), \tag{6}$$

and the contours of $\boldsymbol{G}(\boldsymbol{x}; \boldsymbol{z})$ represents an ellipses with half axes proportional to σ_x and σ_y, rotated an angle θ with respect to the x-axis. Hence this class of functions is believed to incorporate tidal effects.

The parameter vector $\boldsymbol{z}$ is found by minimizing the following nonlinear least square problem; Let $\hat{C}_i$ be the mean CO_2 concentration and Σ_i the standard deviation (calculated from the simulations) in point i, the aim is to minimize

$$f(\boldsymbol{z}) = \sum_{i=1}^{n} f_i(\boldsymbol{z}) = \sum_{i=1}^{n} \left(\frac{\hat{C}_i - \boldsymbol{G}(\boldsymbol{z})_i}{\Sigma_i}\right)^2 \quad i = 1, 2, \ldots, n, \tag{7}$$

where n is the number of grid points. For convenience let $\boldsymbol{F}(\boldsymbol{z}) = [f_1(\boldsymbol{z})\cdots f_n(\boldsymbol{z})]$. Several method for minimizing $f(\boldsymbol{z})$ exists, see for instance Seber and Wild (1989), in this paper the Levenberg–Marquardt method is used (Marquardt, 1963; Levenberg, 1944).

A confidence region, i.e. a region that contains those parameter values with a prescribed probability, here chosen to be 95% probability, can be estimated. Then the covariance matrix, $\textbf{Cov}(\boldsymbol{z}^*)$, for the estimated parameters, $\boldsymbol{z}^*$, is needed, and it can be approximated using the Jacobian, $\boldsymbol{J}(\boldsymbol{z})$,

$$\textbf{Cov}(\boldsymbol{z}^*) \approx (\boldsymbol{J}(\boldsymbol{z}^*)^T \boldsymbol{J}(\boldsymbol{z}^*))^{-1}. \tag{8}$$

where the elements in the Jacobian are given by

$$J_{ij}(\boldsymbol{z}) = \frac{\partial f_i(\boldsymbol{z})}{\partial z_j}, \quad i = 1, 2, \ldots, n; j = 1, \ldots, m, \tag{9}$$

where m is the length of $\boldsymbol{z}$. The covariance matrix is a square matrix, here 3×3, where $diag_j(\textbf{Cov}(\boldsymbol{z}^*))$ is the diagonal element in row j. Using a linear approximation $\boldsymbol{F}(\boldsymbol{z}^* + \Delta \boldsymbol{z}) \approx \boldsymbol{F}(\boldsymbol{z}^*) + \boldsymbol{J}(\boldsymbol{z}^*)\Delta \boldsymbol{z}$ and neglecting cross correlation between parameters, the 95% confidence interval for the estimated parameters

$$z_j \sim z_j^* \pm 1.96 \cdot diag_j(\textbf{Cov}(\boldsymbol{z}^*))^{1/2}, \quad j = 1, 2, 3, \tag{10}$$

where the factor 1.96 is the upper standard normal deviate for the 97.5 percentile point (Aster et al., 2005). Donaldson and Schnabel (1987) compared different types of linearization methods for calculating confidence regions and concluded that the above mentioned method was as good as any of the more complex methods suggested. However, the validity of the linear approximation should be assessed before trusting the resulting confidence values, for instance using curvature measure of nonlinearity (Bates and Watts, 1980). Due to all the other simplifications made, such assessment is not performed here.

The 95% confidence interval of the parameter vector is

$$[\theta, \quad \sigma_x, \sigma_y]$$
$$= [1.2453 \pm 0.2270, 2.0170 \pm 0.2692, 3.3012 \pm 0.4714]. \tag{11}$$

Hence the estimated parameter vector, $\boldsymbol{z}^*$ and the lower and upper bound $\boldsymbol{z}_{\min}$ and $\boldsymbol{z}_{\max}$ are

$$\begin{aligned} \boldsymbol{z}^* &= [1.2453, 2.0170, 3.3012] \\ \boldsymbol{z}_{\min} &= [1.0183, 1.7478, 2.8298] \end{aligned} \tag{12}$$

$$\boldsymbol{z}_{\max} = [1.4723, 2.2862, 3.7726].$$

The resulting ellipse using $\boldsymbol{z}^*$ and $c_0 = 6 \times 10^{-3}$ kg/m^3 is shown in Fig. 2b.

Fig. 3a and b shows the simulated and the approximated CO_2 leakage concentration, as well as the difference between them, along cross sections aligned with the minor and major axes. Note that the approximated concentration is overestimated close to the leakage point, but underestimated further away. It is further noticed that the function used, Eq. (3), is unable to account for the lack of symmetry in the concentration field.

Using $c_0 = 6 \times 10^{-3}$ kg/m^3 and $c_t = 0.226 \times 10^{-3}$ kg/m^3 in Eq. (5), and the parameter vectors in Eq. (12), results in the three ellipses shown in Fig. 4. Changing $z_2 = \sigma_x$ or $z_3 = \sigma_y$ will result in a change
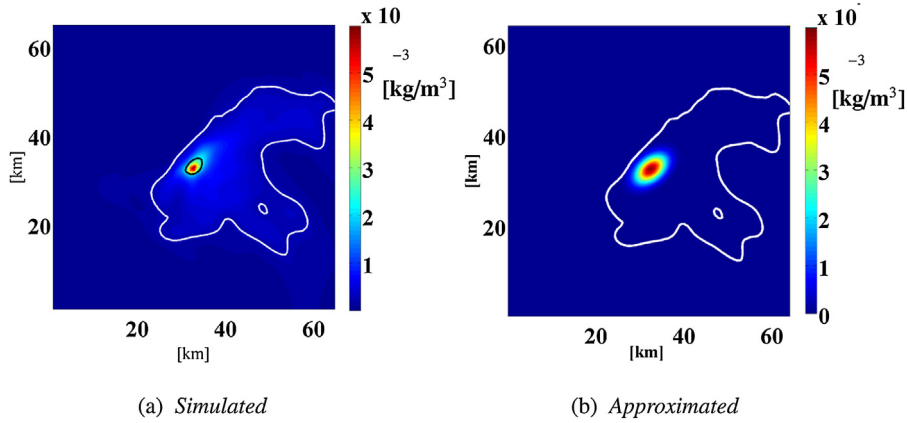
(a) *Simulated*   (b) *Approximated*

Fig. 2. Left: Simulated CO_2 concentration along the seafloor. The white and black contour lines illustrate the area where the concentration is 0.226×10^{-3} and 2.26×10^{-3} kg/m^3, respectively. They represent estimated natural variability and theoretical detection limit, see next section. Right: Least square approximation of the family functions in Eq. (3).
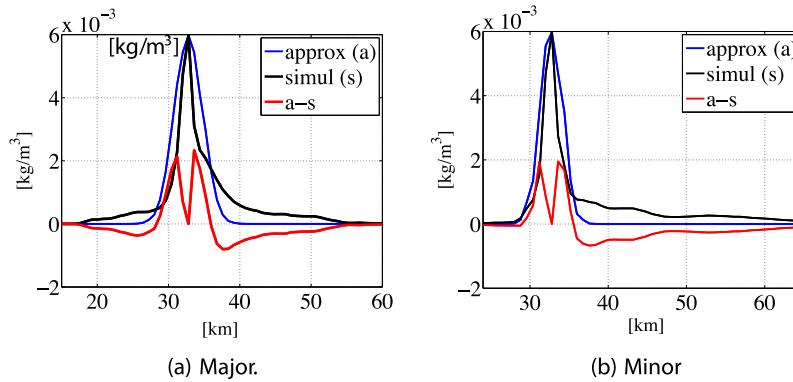

(a) Major.   (b) Minor

Fig. 3. Concentration distribution along the major (left) and minor (right) semi axes of the simulated (black) footprint, the estimated footprint (blue) and the difference between the two (red). (For interpretation of the references to color in this figure legend, the reader is referred to the web version of this article.)

of the area inside of the corresponding ellipse. Changing θ does not represent an area change, but due to the change in direction it is still of great importance regarding sensor placement.

2.3. Quantifying the probability of detecting a leak

Given a leak in the area, the methods from the previous two subsections give us the tools to quantify where and how it will appear. The last thing to establish is the detection limit of the substance in question, i.e. instrument accuracy and statistically significant

Fig. 4. Size and orientation of the three detection ellipses using a concentration of 0.226×10^{-3} kg/m^3.

signal. Once this is in place a cost function can be defined using probability of detection as a metric.

In general, the theoretical precision for measuring total inorganic carbon (c_t) is $\sim 0.090 \times 10^{-3}$ kg/m^3 (Dickson et al., 2007). However; the natural variability, i.e. the seasonal variability in biological production and ocean physics, throughout a season in the North Sea typically varies between 2.260×10^{-3} kg/m^3 and 4.520×10^{-3} kg/m^3 (Omar et al., 2005; Salt et al., 2013). According to Omar et al. (2005) and Botnen et al. (2015) correcting for the natural variability and the anthropogenic trend any additional changes in c_t stems from leakage of CO_2. In the following the threshold of detecting a potential is set to $c_t = 0.226 \times 10^{-3}$ kg/m^3, shown as a white contour line in Fig. 2.

Using the threshold concentration for detection (c_t), the footprint estimation $\mathbf{G}(\mathbf{x}; \mathbf{z})$, Eq. (5), and using $c_0 = 6 \times 10^{-3}$ kg/m^3, the border between the detectable and non-detectable leakage is given by Eq. (6).

A sensor placed at location $\mathbf{x}$ inside this ellipse will detect a leakage at $\mathbf{x}_0$. Due to the assumptions that the parameter vector $\mathbf{z}$ to be independent of leakage location, the problem can readily be inverted; A sensor placed at $\mathbf{x}$ can detect leakage from all points $\mathbf{x}_0$ inside the ellipse, Eq. (6), using $\mathbf{x}_0$ as the independent variable. Summing the probability of leakage inside this detection ellipse results in the probability to detect a leakage if sensor is placed at $\mathbf{x}$.

The optimization problem is hence how to place a number of sensors in a manner that combined have the highest probability of detecting the leak. This is solved using Matlab's built-in genetic algorithm, *ga*, with a population size of 100 individuals. Each
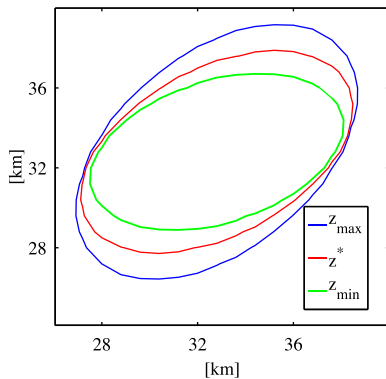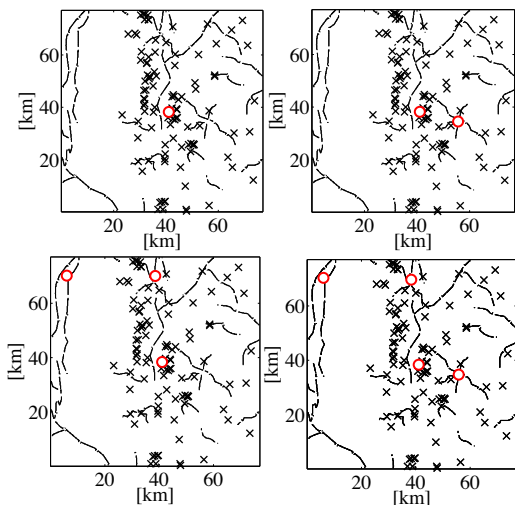
Fig. 5. Optimal placement for one (upper left), two (upper right), three (lower left) and four (lower right) sensors.

individual in the population consists of a position and a detection ellipse for each of the available sensors. The cost function for each individual is the probability of the leak being inside of the sum of detection ellipses. The genetic algorithm will evolve the population toward higher probable detection individuals.

3. Results

Fig. 5 shows the optimal placement of sensors when increasing the number from one to four. The optimal algorithm is not to place the first sensor where the probability of leakage is highest, followed by the second sensor where it is second highest leakage probability and so forth. Several potential leakage locations might be present inside an area covered by a sensor. The figure also illustrates a characteristic of the Genetic Algorithm; notice how the position of the second sensor changes when increasing the number of sensors from two to three. The genetic algorithm only guaranty to give a solution close to global extremum of the cost function. If two close solutions exists other constraints, such as vulnerable areas or cost, determines the sensor layout.

As expected the probability of detecting a leak increases with the number of sensor available, Fig. 6. This figure demonstrates the ability of the procedure to quantify the leak detection capability of a sensor grid, and perform sensitivity analysis caused by parameter and input uncertainties. As the number of sensors increases the three different parameter estimations given in Eq. (12) give increasing relative difference.
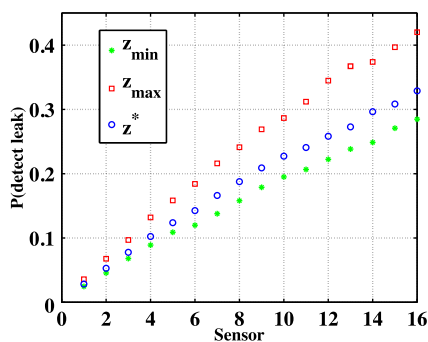

Fig. 6. The probability of detecting a leakage as function of number of sensors. Also showing the sensitivity to parameter uncertainty, see Eq. (12) and Fig. 4.
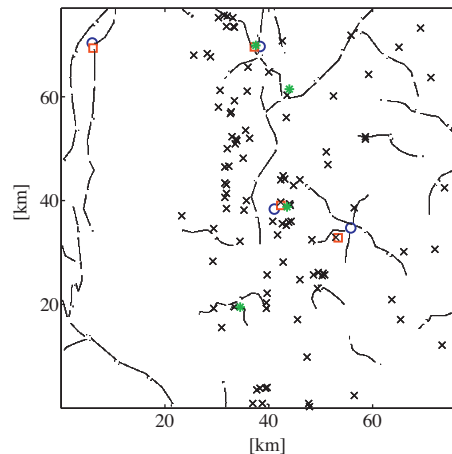

Fig. 7. Placement for four sensor, the blue dots, red squares and green stars show the placement if the z^*, z_{max} and z_{min} parameters, see Eq. (12) and Fig. (4), is used in the detection ellipse. (For interpretation of the references to color in this figure legend, the reader is referred to the web version of this article.)
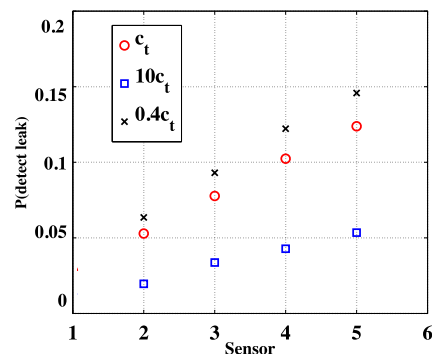

Fig. 8. Comparing detection threshold $c_t = 0.226 \times 10^{-3}$ kg/m^3 (Botnen et al., 2015) with $10c_t$ and $0.4c_t$. The natural variability is represented by $10c_t$ while $0.4c_t$ is the instrumental precision.

Due to the many simplifications and assumptions made the numerical values should be used with caution. However placing sensors in an equally spaced grid gives a 12% probability of detecting leakage using 9 sensors and 22% for 16 sensors, compared to respectively 21% and 32% in an optimal setting. As a consequence, optimal layout of the sensors offers same detection probability using fewer sensors. Fig. 7 shows optimal placement of four sensors for the parameter vectors given in Eq. (12). A change in the estimated parameters does not only change the size of the detection ellipse but also change its rotation, as seen in Fig. 4. When the detection ellipse rotate the sensor will have to move accordingly to monitor the same leakage points.

As a final result, Fig. 8 compare different detection thresholds c_t, $10c_t$ and $0.4c_t$. This demonstrated the need for a proper baseline in order to reduce the detection threshold from $10c_t$, natural variability, to c_t using the procedures in Botnen et al. (2015).

4. Discussion

The monitor design is based on (1) identification of possible seep locations, (2) characteristics of seep to the water column and (3) the ability to detect elevated CO_2 concentrations. The first is a required part of site characterization. The two latter will partially be covered by risk/impact assessments. Presently there is a lack of data and procedures to produce a robust baseline. This study illustrates the necessity of a comprehensive field activity. For instance the

simplified seep characteristics used in Section 2.2 represent a rough estimate based on numerical simulations.

This study does not include spatial dependency on flux rates, small scale mixing and local topography. Further, the symmetry in the detection ellipses does not fully capture the anisotropy of the predicted CO_2 dilution away from the source, Fig. 3. This is necessary simplifications for an efficient inversion from the source to the sensor placement in Section 2.3. Use of more anisotropic functions will have to be addressed in the future, Eq. (3).

One of the purposes of the monitoring program will be to increase the quality of the baseline by adding new data. For instance, long time series will reduce uncertainties in all scenario predictions. Together with better calibration of sensors, the detection threshold can be reduced, resulting in increased detection probability, Fig. 8.

There may be several combinations of sensor placement that give almost equal detection probability. Constrains can lead to choosing a layout other than the optimal solution, such as for instance investment and operational cost. Some of these might be included in the cost function.

Acknowledgements

References

Alendal, G., Berntsen, J., Engum, E., Furnes, G.K., Kleiven, G., Eide, L.I., 2005. Influence from 'ocean weather'on near seabed currents and events at Ormen Lange. Mar. Petrol. Geol. 22, 21–31.

Alendal, G., Dewar, M., Ali, A., Evgeniy, Y., Vielstädte, L., Avlesen, H., Chen, B., 2013. Technical Report on Environmental Conditions and Possible Leak Scenarios in the North Sea. Technical Report D3.4. ECO_2 Deliverables. http://www.eco2-project.eu

Alendal, G., Drange, H., 2001. Two-phase, near-field modeling of purposefully released CO_2 in the ocean. J. Geophys. Res. 106.

Aster, R.C., Borchers, B., Thurber, C.H., 2005. Parameter Estimation and Inverse Problems. Elsevier Academic Press, ISBN 0-12-065604-3.

Bates, D., Watts, D., 1980. Relative curvature measures of nonlinearity. J. R. Stat. Soc. Ser. B Methodol 42, 1–25.

Blackford, J.C., Widdicombe, S., Bickle, M.J., Lowe, D., Chen, B., 2010. Environmental risks and performance assessment of carbon dioxide (CO_2) leakage in marine ecosystems. In: Developments and Innovation in Carbon Dioxide (CO_2) Capture and Storage Technology, Vol. 2 – Carbon Dioxide (CO_2) Storage and Utilisation. Woodhead Publishing Limited, pp. 344–373.

Boait, F.C., White, N.J., Bickle, M.J., Chadwick, R.A., Neufeld, J.A., Huppert, H.E., 2012. Spatial and temporal evolution of injected CO_2 at the Sleipner Field, North Sea. J. Geophys. Res. Solid Earth (1978–2012), 117.

Botnen, H., Omar, A., Thorseth, I., Johannessen, T., Alendal, G., 2015. The effect of submarine CO_2 vents on seawater: implications for detection of subsea carbon sequestration leakage. Limnol. Oceanogr. 60, 402–410.

Boyd, A.D., Liu, Y., Stephens, J.C., Wilson, E.J., Pollak, M., Peterson, T.R., Einsiedel, E., Meadowcroft, J., 2013. Controversy in technology innovation: contrasting media and expert risk perceptions of the alleged leakage at the Weyburn carbon dioxide storage demonstration project. Int. J. Greenh. Gas Control 14, 259–269.

Brewer, P.G., Chen, B., Warzinki, R., Baggeroer, A., Peltzer, E.T., Dunk, R.M., Walz, P., 2006. Three-dimensional acoustic monitoring and modeling of a deep-sea CO_2 droplet cloud. Geophys. Res. Lett. 33, 5.

Caldeira, K., Wickett, M.E., 2003. Oceanography: anthropogenic carbon and ocean pH. Nature 425, 237.

Davies, A.M., Furnes, G.K., 1980. Observed and computed M_2 tidal currents in the North Sea. J. Phys. Oceanogr. 10, 237–257.

Dewar, M., Sellami, N., Chen, B., 2014. Dynamics of rising CO_2 bubble plumes in the QICS field experiment. Int. J. Greenh. Gas Control, http://dx.doi.org/10.1016/j.ijggc.2014.11.003.

Dewar, M., Wei, W., McNeil, D., Chen, B., 2013. Small-scale modelling of the physiochemical impacts of CO_2 leaked from sub-seabed reservoirs or pipelines within the North Sea and surrounding waters. Mar. Pollut. Bull.

Dickson, A., Sabine, C., Christian, J.E., 2007. Guide to best practices for ocean CO_2 measurements. PICES Spec. Publ. 3.

Donaldson, J., Schnabel, R., 1987. Computational experience with confidence regions and confidence intervals for nonlinear least squares. Technometrics 29, 67–82.

EU Commission, 2011. Implementation of Directive 2009/31/EC on the Geological Storage of Carbon Dioxide, CO_2 Storage Life Cycle Risk Management Framework. Guidance Document 2.

Haugan, P.M., Joos, F., 2004. Metrics to assess the mitigation of global warming by carbon capture and storage in the ocean and in geological reservoirs. Geophys. Res. Lett. 31, L18202.

Levenberg, K., 1944. A method for the solution of certain non-linear problems in least squares. Quart. J. Appl. Math. II, 164–168.

Marquardt, D.W., 1963. An algorithm for least-squares estimation of nonlinear parameters. J. S. Ind. Appl. Math. 11, 431–441.

Mellor, G., Yamada, T., 1982. Development of a turbulence closure model for geophysical fluid problems. Rev. Geophys. Space Phys. 20, 851–875.

Noble, R.R.P., Stalker, L., Wakelin, S.A., Pejcic, B., Leybourne, M.I., Hortle, A.L., Michael, K., 2012. Biological monitoring for carbon capture and storage – a review and potential future developments. Int. J. Greenh. Gas Control 10.

Nooner, S., Zumberge, M., Eiken, O., Stenvold, T., Thibeau, S., 2006. Constraining the density of CO_2 within the Utsira formation using time-lapse gravity measurements. Miscellaneous.

Norwegian Petroleum Directorate, 2014. Factmap. http://www.npd.no/en/Maps/Fact-maps/

Oldenburg, C.M., Lewicki, J.L., 2006. On leakage and seepage of CO_2 from geologic storage sites into surface water. Environ. Geol. 50, 691–705.

Omar, A., Johannessen, T., Bellerby, R.G., Olsen, A., Anderson, L.G., Kivimäe, C., 2005. Sea ice and brine formation in Storfjorden: implications for the Arctic winter time air–sea CO_2 flux. In: The Nordic Seas: An Integrated Perspective., pp. 177–187.

Rutqvist, J., 2012. The Geomechanics of CO_2 Storage in Deep Sedimentary Formations. Geotechnical and Geological Engineering 30, 525–551.

Salt, L.A., Thomas, H., Prowe, A., Borges, A.V., Bozec, Y., Baar, H.J., 2013. Variability of North Sea pH and CO_2 in response to North Atlantic oscillation forcing. J. Geophys. Res.: Biogeosci. 118, 1584–1592.

Seber, G.A.F., Wild, C.J., 1989. Nonlinear regression. In: Wiley Series in Propability Statistics, ISBN 0-471-47135-6.

Wegener, G., Shovitri, M., Knittel, K., Niemann, H., Hovland, M., Boetius, A., 2008. Biogeochemical processes and microbial diversity of the Gullfaks and Tommeliten methane seeps (Northern North Sea). Biogeosci. Discuss. 5, 971–1015.